Journal of Sound and Vibration 327 (2009) 231–248

Contents lists available at ScienceDirect

Journal of Sound and Vibration

journal homepage: www.elsevier.com/locate/jsvi

Nonlinear vibrations of a radially stretched circular hyperelastic membrane

Paulo B. Gonçalves *, Renata M. Soares, Djenane Pamplona

Department of Civil Engineering, Catholic University, PUC-Rio, Rio de Janeiro 22451-900, Brazil

ARTICLE INFO

Article history:
Received 28 October 2008
Received in revised form
30 May 2009
Accepted 25 June 2009
Handling Editor: C.L. Morfey
Available online 21 July 2009

ABSTRACT

This paper presents a detailed analysis of the nonlinear vibration response of a pre-stretched hyperelastic membrane subjected to finite deformations and a time-varying lateral pressure. The problem is both geometrically and materially nonlinear due to finite deformations and a hyperelastic constitutive relationship. The membrane material is assumed to be isotropic, homogeneous, and neo-Hookean. First, the exact solution of the membrane under a uniform radial stretch is obtained. The equations of motion of the pre-stretched membrane are then derived. From the linearized equations, the natural frequencies and mode shapes of the membrane are analytically obtained. The natural modes are then used to approximate the nonlinear deformation field using the Galerkin method. Several reduced order models are tested and compared with the results evaluated for the same membrane using a nonlinear finite element formulation. Excellent agreement is observed. The results show the strong influence of the stretching ratio on the linear and nonlinear oscillations of the membrane. Finally, the influence of the constitutive law on linear and nonlinear vibrations is investigated. Results show that several constitutive laws for hyperelastic rubber-like materials lead to the same frequency–amplitude relation.

1. Introduction

Membranes have received considerable attention in recent years due to their applicability in numerous engineering areas, including space applications, actuators, sensors, robotics, bioengineering devices, and civil engineering structures. A review of the literature on the static and dynamic behavior of membranes, hyperelastic or not, theoretical and experimental, with emphasis in practical applications, can be found in Jenkins and Leonard [1], Jenkins [2], and Jenkins and Korde [3]. In addition, membranes play a significant role in nature [4,5]. In recent years, intensive research has been conducted on the development of new membrane materials, including shape memory polymers [6,7] and dielectric elastomers [8–12]. These advanced materials are of interest for use in sensors and vibration control [13,14], bioengineering [15–17], and thin-films used in compliant microdevices [6].

The analysis of membrane mechanics is an important topic in nonlinear continuum mechanics. In particular, the study of hyperelastic membranes under finite deformations, such as elastomeric membranes and most biological tissues, is a rather challenging subject, and in such cases, elasticity in the fully nonlinear range must be employed. The pioneering works of Rivlin and co-workers [18,19] on nonlinear elasticity is the basis for the analysis of structures under large deformations. The first developments in this field are collected in the classical work by Green and Adkins [20].

* Corresponding author. Tel.: +55 21 3527 1188; fax: +55 21 3527 1195.
E-mail address: paulo@puc-rio.br (P.B. Gonçalves).

0022-460X/$ - see front matter © 2009 Elsevier Ltd. All rights reserved.
doi:10.1016/j.jsv.2009.06.023

Recent advances in finite elasticity and useful historical reviews can be found in Libai and Simmonds [21] and Fu and Ogden [22]. A key point in the analysis of hyperelastic membranes using the theory of finite elasticity is the choice of an appropriate strain-energy density function. Strain-invariant constitutive models are usually used to describe the behavior of hyperelastic materials. The simplest constitutive model is the neo-Hookean model, which can be viewed as a simplification of the Mooney–Rivlin law. These two constitutive laws are widely used in the literature. In addition to these classical models, Ogden [23,24], Yeoh [25], and Arruda and Boyce [26], among others, have proposed useful constitutive models for the analysis of rubber-like materials. The reader may refer to the works by Selvadurai [27] and Saccomandi and Ogden [28] for critical reviews on constitutive models for hyperelastic materials.

The mechanical behavior of biomembranes is usually described via a Fung-type exponential pseudostrain energy function and similar constitutive laws [4,5]. The mechanical analysis of membranes may provide insight into the analysis of several clinical procedures and biological phenomena, including cataract surgery, the formation of aneurysms, and balloon angioplasty [29,30].

After half a century of fruitful research, the equilibrium and stability analysis of hyperelastic membranes continues to be a topic of interest in applied mechanics [31–35]. This paper considers the nonlinear vibrations of a pressure loaded, initially flat, pre-stretched circular membrane. Plane deformation of a hyperelastic membrane is one of the classical problems in the theory of finite elasticity. Several examples are found in the studies by Rivlin and Saunders [36] and Green and Adkins [20]. In addition, Wong and Shield [37] studied the plane deformations of neo-Hookean membranes, and showed that under large meridional strains, the nonlinear problem can be reduced to a linear one. Radial deformations of a plane sheet containing a circular hole or inclusion were studied by Verna and Rana [38]. The inflation of a circular membrane by lateral pressure is another problem of interest in finite elasticity, and has been important in the development of constitutive equations and the identification of material parameters. Treloar [39] carried out such membrane inflation experiments, and measured the deformed profiles and stretch ratio distributions in a rubber membrane at different inflation levels. Adkins and Rivlin [40] used the theory of nonlinear elastic membranes to calculate the inflated profiles for several forms of the strain-energy function and compared the results with the data obtained by Treloar [39]. Campbell [41] studied an initially tensioned circular membrane subject to uniform pressure. Studies on the inflation of a flat circular membrane employing different strain-energy functions were performed by Klingbeil and Shield [42], Hart-Smith and Crisp [43], Foster [44], and Tielking and Feng [45], among others, who used the minimum potential energy principle to study the axi-symmetric deformation of a pressure loaded circular membrane with a rigid inclusion. Wineman et al. [46] showed how the measured profiles and stretch ratio distributions could be used as part of a material identification method to determine the form of the strain-energy function. Recently, a circular membrane was inflated to determine properties of elastomers by Przybylo and Arruda [47], and of several polymeric materials by Li et al. [48] and Rachik et al. [49] measured the properties of several other polymeric materials. Wineman and Shaw [50] studied the influence of thermally induced scissions of macromolecular networks and their subsequent crosslinking on the post-scission inflation of a circular elastomeric membrane.

The linear vibration analysis of membranes (drumheads) using the wave equation is a classical problem in mechanics and applied mathematics [51]; however, several aspects of this problem remain for further research [52,53]. The nonlinear small-amplitude vibrations of elastic membranes have also been investigated [54,55]. There are fewer studies on the analysis of the linear, and particularly the nonlinear, vibrations of hyperelastic membranes [1,3,9,56–63].

Therefore, the aim of the present work is to study the linear and nonlinear vibrations of a pre-stretched circular hyperelastic membrane, with emphasis on a few important nonlinear characteristics, such as frequency–amplitude and resonance curves, bifurcation diagrams, and basins of attraction. A detailed parametric analysis shows the influence of the initial radial traction on the linear and nonlinear vibrations of the membrane. The membrane material is assumed to be isotropic and incompressible, and its behavior is described by the neo-Hookean constitutive law. These hypotheses have been widely used to describe the behavior of elastomers.

A variational formulation, considering finite deformations, is used to derive the equilibrium equations of the membrane under a uniform radial stretch and the equations of motion of the pre-stretched membrane. The linear and nonlinear vibrations are analyzed, and the influence of the pre-stretch on these results is evaluated. The problem is also analyzed using the finite element software Abaqus 6.5® [64]. Finally, the influence of the constitutive law on the frequency–amplitude relation is also investigated.

2. Problem formulation

2.1. Hyperelastic membrane theory

This work considers a homogeneous, isotropic, circular hyperelastic membrane of undeformed radius R_o, thickness h, and mass density Γ. It is assumed that $h/R_o \ll 1$ so that the deformed membrane can be described by the theory of hyperelastic membranes under finite deformations [20].

The major aspects of the theory used in this work are outlined below. For a conservative system, the elastic Cauchy stresses are derived from a strain-energy density function per unit undeformed volume W that is a function of the deformation tensors. Thus, given an undeformed reference state, the strain-energy density may be described in terms of

three independent quantities, namely the principal stretches λ_1, λ_2, and λ_3, or alternatively, the strain invariants I_1, I_2, and I_3:

$$W = W(\lambda_1, \lambda_2, \lambda_3) = W(I_1, I_2, I_3) \tag{1}$$

The three strain invariants of the deformation field can be written in terms of the principal stretches λ_i $(i = 1, 2, 3)$ as

$$\begin{aligned} I_1 &= \lambda_1^2 + \lambda_2^2 + \lambda_3^2 \\ I_2 &= (\lambda_1\lambda_2)^2 + (\lambda_2\lambda_3)^2 + (\lambda_1\lambda_3)^2 \\ I_3 &= (\lambda_1\lambda_2\lambda_3)^2 \end{aligned} \tag{2}$$

Rubber-like materials exhibit very small volume changes [65], so incompressibility is usually assumed for simplicity. If the material is incompressible, $I_3 = 1$, and the strain-energy density is a function of the first two strain invariants in (2).

The stress components can be determined after choosing the constitutive law. There are several constitutive laws in literature particularly adapted to the representation of elastomers written in terms of the strain invariants. In this study, the neo-Hookean constitutive model for the energy density function is initially adopted, and for an incompressible material is given by

$$W = C_1(I_1 - 3) \tag{3}$$

where C_1 is a material parameter. This equation provides a simple but realistic model for a rubber-elastic type material [27,33,34,65]. The neo-Hookean material description reduces to linear elasticity with a Poisson's ratio of $v = \frac{1}{2}$ for small strains. The best constitutive law always depends on the deformation range considered in the analysis and on the membrane material. More refined constitutive laws are considered in Section 5.

Consider an isotropic elastic material, which undergoes finite elastic deformations so that a particle initially at a position P_o in a rectangular Cartesian reference system X_i, moves to position P in a rectangular Cartesian reference system x_i, as illustrated in Fig. 1, where the deformed and undeformed configurations, basic geometric parameters, and associated coordinate systems are depicted.

The coordinates of a material particle at a point P_o on the mid-surface undeformed reference configuration, in a coordinate system with the origin at the center of the circular membrane, are given by

$$\begin{aligned} X_1 &= \rho \cos\theta \\ X_2 &= \rho \sin\theta \\ X_3 &= 0 \end{aligned} \tag{4}$$

where ρ, θ, and X_3 are the radial, circumferential, and transversal coordinates, respectively.

The coordinates of the same typical point P at a given instant t, in an arbitrary deformed configuration are given by

$$\begin{aligned} x_1 &= r(\rho, \theta, t)\cos\beta(\rho, \theta, t) \\ x_2 &= r(\rho, \theta, t)\sin\beta(\rho, \theta, t) \\ x_3 &= z(\rho, \theta, t) \end{aligned} \tag{5}$$

where r, β, and z are the radial, circumferential, and transversal coordinates of the deformed membrane, respectively. The coordinates ρ and θ and time t are taken as independent variables.

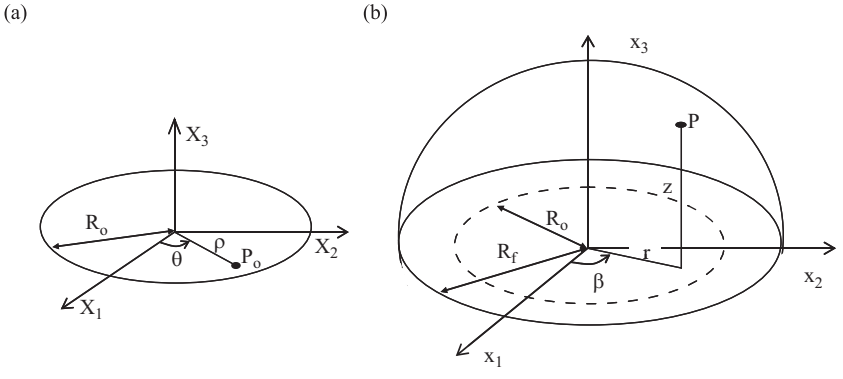

Fig. 1. (a) Undeformed and (b) deformed configurations of the membrane, geometric parameters and associated coordinate systems.

Since this analysis is on the dynamic nonlinear behavior of a pre-stretched membrane, the coordinates of a deformed point are

$$\begin{aligned} r(\rho,\theta,t) &= r_o(\rho,\theta) + u(\rho,\theta,t) \\ \beta(\rho,\theta,t) &= \theta + \beta_o(\rho,\theta) + v(\rho,\theta,t) \\ z(\rho,\theta,t) &= z_o(\rho,\theta) + w(\rho,\theta,t) \end{aligned} \tag{6}$$

where (see Fig. 2) $w(\rho,\theta,t)$, $u(\rho,\theta,t)$ and $v(\rho,\theta,t)$ are the perturbation components in the radial, transversal and circumferential directions, respectively and $r_o(\rho,\theta)$, $z_o(\rho,\theta)$ and $\beta_o(\rho,\theta)$ describes the initial deformed static state.

The principal stretches are defined as

$$\lambda_i = \frac{dS_i}{ds_i} \tag{7}$$

where dS_i and ds_i, are the deformed and undeformed lengths, respectively, of an infinitesimal element in the principal direction.

Thus, considering Eq. (7), the in-plane principal stretches are given by

$$\lambda_1 = \sqrt{r_{,\rho}^2 + r^2\phi_{,\rho}^2 + z_{,\rho}^2} \tag{8}$$

$$\lambda_2 = \frac{\sqrt{r_{,\theta}^2 + r^2\phi_{,\theta}^2 + z_{,\theta}^2}}{\rho} \tag{9}$$

where $\partial(\ )/\partial\rho = (\ )_{,\rho}$ and $\partial(\ )/\partial\theta = (\ )_{,\theta}$.

The principal stretch in the normal direction λ_3, taking into account the incompressibility condition $\lambda_1\lambda_2\lambda_3 = 1$, is given by

$$\lambda_3 = \frac{1}{\lambda_1\lambda_2} \tag{10}$$

or, physically:

$$\lambda_3 = \frac{H}{h} \tag{11}$$

where H is the deformed membrane thickness.

Thus, the strain invariant I_1 is given by

$$\begin{aligned} I_1 = \sum_{i=1}^{3}\lambda_i^2 &= r_{,\rho}^2 + r^2\beta_{,\rho}^2 + z_{,\rho}^2 + r_{,\theta}^2 + r^2\beta_{,\theta}^2 + z_{,\theta}^2/\rho^2 \\ &+ \frac{\rho^2}{(r_{,\rho}^2 + r^2\beta_{,\rho}^2 + z_{,\rho}^2)(r_{,\theta}^2 + r^2\beta_{,\theta}^2 + z_{,\theta}^2) - (r_{,\rho}r_{,\theta} + r^2\beta_{,\rho}\beta_{,\theta} + z_{,\rho}z_{,\theta})^2} \end{aligned} \tag{12}$$

The last term in (12) corresponds to λ_3^2, and generates the nonlinear terms in the equilibrium equations.

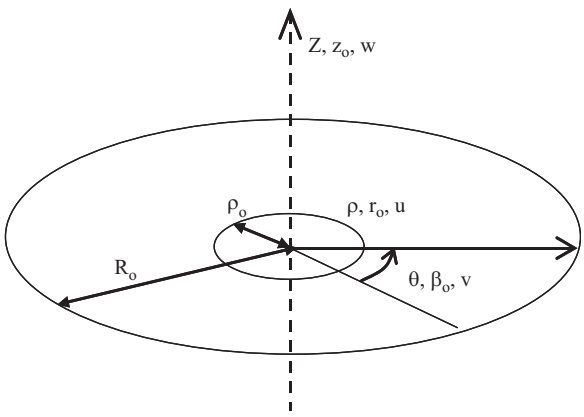

Fig. 2. Static and dynamic components in the cylindrical coordinate system.

The elastic strain energy U, is the volume integral of W in the undeformed configuration, which in the present case becomes

$$U = \int_0^{R_o} \int_0^{2\pi} \int_0^{h} W(r, r_{,\rho}, r_{,\theta}, z, z_{,\rho}, z_{,\theta}, \beta, \beta_{,\rho}, \beta_{,\theta}, \rho, \theta)\rho \, dz \, d\theta \, d\rho \tag{13}$$

The pressure potential energy is the product of the pressure by the integral of the deflection on the membrane [45,66]. We must rigorously evaluate the exact volume of the membrane by taking into account both the transversal and in-plane displacements. One possible approximation is to assume that the pressure works only on the transversal component. In this case, the pressure vector is assumed to be parallel to z during the inflation, and is not normal to the membrane. This approximation slightly affects the shape of the membrane and gives a less rounded surface. Of course, such an approximation is only valid if the in-plane displacement components are small.

The work term W_e, considering a radial stretch due to a uniform distributed force f along the circular boundary, and a uniform pressure $p_h(t)$, is

$$W_e = 2\pi\rho f(r_o - \rho)|_{\rho=R_o} + p_h(t)\Delta V \tag{14}$$

where $\Delta V = V_f - V_o$ is the variation of the volume enclosed by the structure due to the pressure, V_f is the volume enclosed by the deformed membrane, and V_o is the volume enclosed by the undeformed structure. Since the membrane is initially flat, $V_o = 0$.

The kinetic energy T is given by

$$T = \int_0^{R_o} \int_0^{2\pi} \int_0^{h} \Gamma \frac{(\dot{u}^2 + \dot{v}^2 + \dot{w}^2)}{2} \rho \, dz \, d\theta \, d\rho \tag{15}$$

where Γ is the mass density of the material in the natural configuration, and $\dot{(\,)} = \partial(\,)/\partial t$. Due to the incompressibility condition, the mass density remains constant during the deformation process.

Similar formulations for other material behaviors based on strain invariant constitutive laws, such as Mooney–Rivlin material, can be derived in a very straightforward manner by modifying the strain-energy density given by Eq. (3). The influence of different constitutive laws is analyzed in Section 5.

3. Static analysis

The membrane is first uniformly stretched in the radial direction, reaching a final radius R_f, and then fixed along the edge. The equations derived in the previous section can be specialized to solve this problem. Since only axi-symmetric deformations are considered, all variables are independent of the circumferential coordinate θ. Because the deformation is axially symmetric, the principal directions of stretch are known *a priori* to be in the meridional, circumferential, and normal directions, relative to the deformed surface. Denoting the meridional direction as (1) the circumferential direction as (2) and the normal direction as (3) the principal stretches are given by

$$\lambda_1 = \frac{dr_o}{d\rho} \quad \lambda_2 = \frac{r_o}{\rho} \quad \lambda_3 = \frac{\rho}{r_o r_{o,\rho}} \tag{16}$$

and the strain energy reduces to

$$U = \int_0^{R_o} \int_0^{2\pi} C_1 h \left[r_{o,\rho}^2 + \frac{r_o^2}{\rho^2} + \frac{\rho^2}{r_o^2 r_{o,\rho}^2} - 3 \right] \rho \, dz \, d\theta \, d\rho \tag{17}$$

Here, the membrane equations are obtained by directly minimizing the total potential energy. From Eqs. (17) and (14), the following nonlinear differential equilibrium equation in terms of the radial coordinate function-$r_o(\rho)$ is obtained:

$$\frac{r_o}{\rho} - \frac{3\rho^3}{r_o^3 r_{o,\rho}^2} - r_{o,\rho} - \rho r_{o,\rho\rho} + \frac{3\rho^2}{r_o^2 r_{o,\rho}^3} - \frac{3\rho^3 r_{o,\rho\rho}}{r_o^2 r_{o,\rho}^4} = 0 \tag{18}$$

and the associated boundary condition is

$$r_o(R_o) = R_f \tag{19}$$

The exact solution of Eq. (18) that satisfies the boundary condition (19) is

$$r_o(\rho) = \delta\rho \tag{20}$$

where $\delta = R_f/R_o$ is the radial stretch ratio. The static transversal and circumferential displacement components, z_o and β_o, are zero.

Therefore, the principal stresses and stretches are given, respectively, by

$$\sigma_1 = \sigma_2 = \frac{2C_1(\delta^6 - 1)}{\delta^4} \tag{21.a}$$

$$\lambda_1 = \lambda_2 = \delta, \quad \lambda_3 = 1/\delta^2 \tag{21.b}$$

4. Dynamic analysis

The stretched membrane is next subjected to a transversal time-varying pressure, and its nonlinear vibrations are analyzed. The total displacement field with respect to the undeformed configuration is given by

$$\begin{aligned} r(\rho,\theta,t) &= \delta\rho + u(\rho,\theta,t) \\ \beta(\rho,\theta,t) &= v(\rho,\theta,t) \\ z(\rho,\theta,t) &= w(\rho,\theta,t) \end{aligned} \tag{22}$$

Substituting (22) into Eqs. (13)–(15) gives the Lagrange function

$$L = T - U + W_e \tag{23}$$

in terms of u, v, and w.

The nonlinear equations of motion are then obtained by applying Halmilton's principle. They are:

$$\rho\frac{\partial W}{\partial r} - \frac{\partial}{\partial\rho}\left(\frac{\partial W}{\partial r_{,\rho}}\right) - \frac{\partial}{\partial\theta}\left(\frac{\partial W}{\partial r_{,\theta}}\right) + \rho\Gamma\frac{\partial^2 u}{\partial t^2} - \zeta\frac{\partial u}{\partial t} = 0 \tag{24.a}$$

$$\frac{\partial W}{\partial\beta} - \frac{\partial}{\partial\rho}\left(\frac{\partial W}{\partial\beta_{,\rho}}\right) - \frac{\partial}{\partial\theta}\left(\frac{\partial W}{\partial\beta_{,\theta}}\right) + \rho\Gamma\frac{\partial^2 v}{\partial t^2} - \zeta\frac{\partial v}{\partial t} = 0 \tag{24.b}$$

$$\frac{\partial W}{\partial z} - \frac{\partial}{\partial\rho}\left(\rho\frac{\partial W}{\partial z_{,\rho}}\right) - \frac{\partial}{\partial\theta}\left(\rho\frac{\partial W}{\partial z_{,\theta}}\right) + \rho\Gamma\frac{\partial^2 w}{\partial t^2} - \zeta\frac{\partial w}{\partial t} = 0 \tag{24.c}$$

where $\zeta = c/C_c$ is the damping ratio and C_c is the linear critical damping.

The uniformly distributed hydrostatic pressure is given by

$$p_h(t) = P_o\cos(\Omega t) \tag{25}$$

where P_o is the excitation magnitude and Ω is the excitation frequency.

4.1. Linear free vibration analysis

Linearizing Eqs. (24.a)–(24.c), the in-plane equations are decoupled from the equation in the transversal direction. By taking Eq. (20) into account and ignoring the damping and external load, the following linearized equation of motion in the transversal direction is obtained:

$$\frac{\partial^2 w}{\partial t^2} = \frac{2C_1}{\Gamma}\left(\frac{1}{\delta^6} - 1\right)\left(\frac{\partial^2 w}{\partial\rho^2} + \frac{1}{\rho}\frac{\partial w}{\partial\rho} + \frac{1}{\rho^2}\frac{\partial^2 w}{\partial\theta^2}\right) \tag{26}$$

which is similar to the classical wave equation if

$$\mathbf{c}^2 = \frac{2C_1}{\Gamma}\left(\frac{1}{\delta^6} - 1\right) \tag{27}$$

The free vibration modes are obtained by solving Eq. (26) together with the relevant boundary and continuity conditions. These are:

$$w(\rho,\theta,t) = A_{mn}J_n\left(\alpha_{mn}\frac{\rho}{R_o}\right)\cos(n\theta)\cos(\omega_{mn}t) \tag{28}$$

where A_{mn} is the modal amplitude; n is the number of waves of the vibration mode in the circumferential direction; J_n is the Bessel function of the first kind and order n; α_{mn} are the zeros of the Bessel function J_n numbered in the order of increasing magnitudes ($m = 1,2,3,\ldots,\infty$, is the number of the zero); ω_{mn} is the natural (circular) frequency of the (m,n) mode. The natural frequencies of the stretched hyperelastic membrane are given by

$$\omega_{mn} = \alpha_{mn}\sqrt{\frac{2C_1(\delta^6 - 1)}{R_o^2\delta^6\Gamma}} \tag{29}$$

If the limit $\delta \to \infty$ in (20) is taken, one can conclude that as the stretching ratio increases, the frequencies converge asymptotically to

$$\omega_{mn_{(\delta\to\infty)}} = \alpha_{mn}\sqrt{\frac{2C_1}{R_o^2\Gamma}} \tag{30}$$

4.1.1. Linear vibration results

A circular membrane with initial radius $R_o = 1\,\text{m}$, thickness $h = 0.001\,\text{m}$, and mass density $\Gamma = 2200\,\text{kg/m}^3$ is considered for the numerical analysis. The constant of the neo-Hookean material is $C_1 = 0.17\,\text{MPa}$. The adopted stress–strain relation and material constant were obtained experimentally and are given in [27]. Fig. 3 shows the variation of the natural frequencies as a function of the wavenumbers m and n for a stretching ratio $\delta = 1.10$. For a given value of n, the frequencies increase linearly with m, while the variation of frequencies with n for a given value of m is slightly nonlinear. The influence of the stretching ratio δ on the natural frequencies is illustrated in Fig. 4 for the three lowest natural frequencies, and the corresponding vibration modes are shown in Fig. 5. The frequencies increase quickly from zero

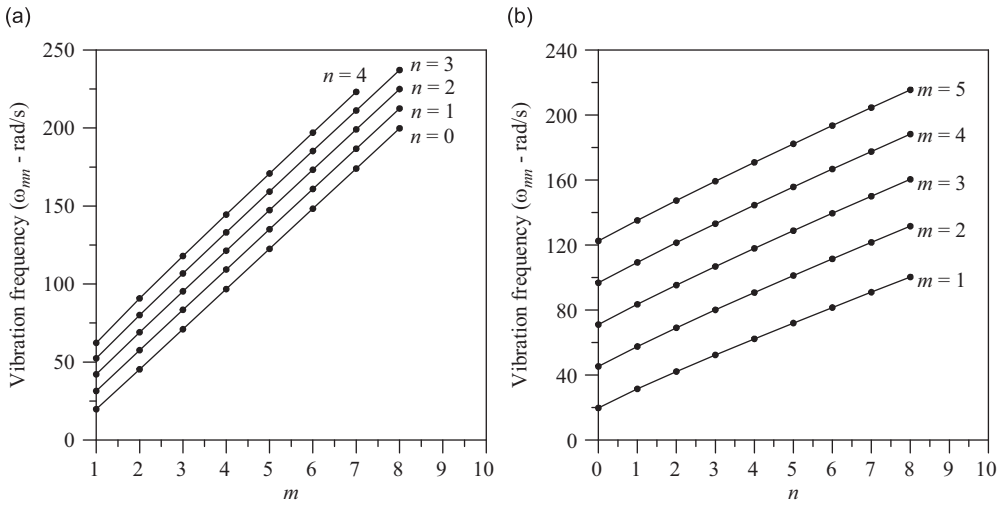

Fig. 3. Variation of the natural frequencies with the wavenumbers (a) m and (b) n, $\delta = 1.10$.

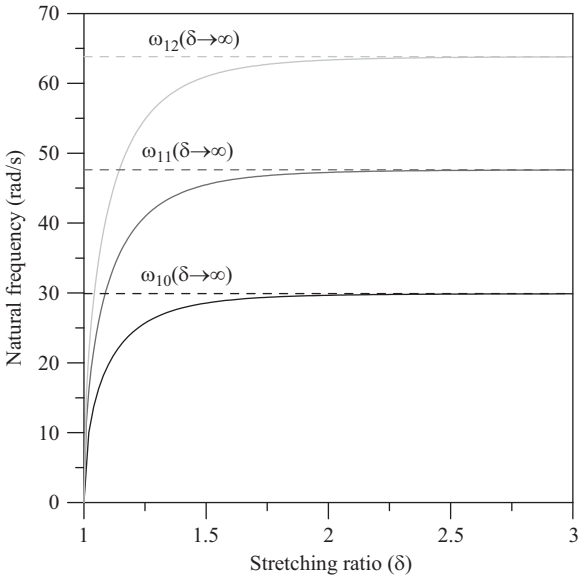

Fig. 4. Variation of the natural frequencies with the radial stretching ratio δ.

as δ increases from 1 (unstretched configuration), and tend to the upper bound given by Eq. (30) for $\delta > 2$. The dashed lines denote the upper bounds. All frequencies display similar behavior. The linear frequencies are independent of the initial membrane thickness h.

To help in the derivation of an accurate low dimensional model for the free and forced finite amplitude nonlinear vibration analysis of the membrane, the convergence of the natural frequencies and modes shapes is first analyzed using the finite element software Abaqus 6.5®. Solid, shell, and membrane elements were tested. Convergence of the natural frequencies up to three decimal places can be obtained using the membrane elements M3D4 or M3D3 and a mesh of 9789 elements. The stretched configuration is accomplished by imposing an initial uniform radial displacement along the boundary ($R_f = \delta R_o$) in the FE program. Then, the dynamic analysis is performed considering the initially stretched membrane fixed along the boundary. The vibration modes and frequencies are computed for increasing values of the stretching ratio δ. The finite element (FEM) results for the natural frequencies are compared with the analytical results (AN), Eq. (29), in Table 1. The FE frequencies are computed using the subspace iteration method and the Q-R algorithm [64].

4.2. Nonlinear vibration analysis

First, the nonlinear free vibration response of the membrane under large and small-amplitude vibrations is obtained using the FE method. The free vibration displacement components u, v, and w along the deformed radius of the membrane ($\delta = 1.10$) for a typical large amplitude axi-symmetric configuration are illustrated in Fig. 6. The numerical results show

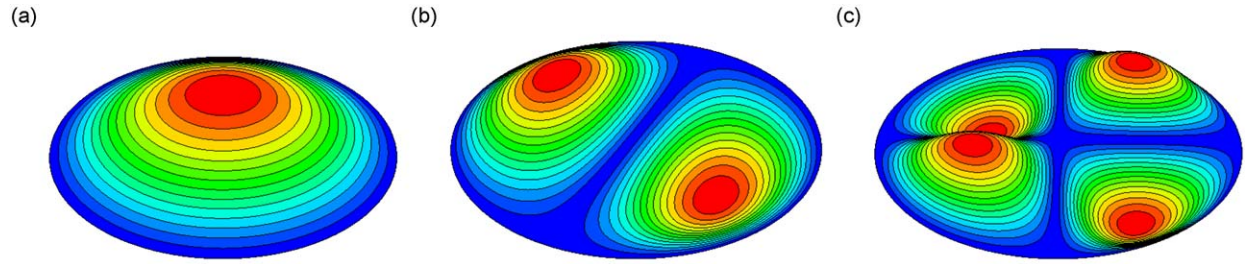

Fig. 5. The three lowest vibration modes of the circular membrane. (a) $m = 1$; $n = 0$; (b) $m = 1$; $n = 1$; (c) $m = 1$; $n = 2$.

Table 1
Vibration frequencies (rad/s).

m	n	$\delta = 1.10$			$\delta = 1.50$			$\delta = 2.0$		
		FEM	AN	%	FEM	AN	%	FEM	AN	%
1	0	19.729	19.729	0.0	28.551	28.551	0.0	29.456	29.663	0.697
1	1	31.441	31.435	−0.019	45.503	45.498	−0.011	47.268	47.262	−0.013
1	2	42.141	42.235	0.222	60.977	60.978	0.002	63.359	63.341	−0.028

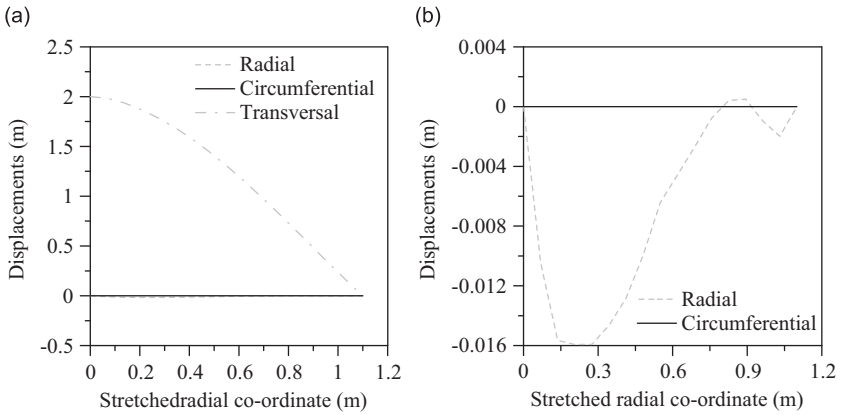

Fig. 6. (a) Variation of the displacements of the pre-stretched membrane under large amplitude vibrations along the deformed radius ($\delta = 1.1$). (b) Magnification of the in-plane displacements.

that during the transversal vibrations, the in-plane components u and v are negligible compared with the transversal displacement w. Similar results are found for the forced vibrations of the membrane under pressure load. For derivation of a low dimensional model for the nonlinear transversal vibrations of the membrane, the in-plane displacements u and v are neglected and Eq. (24.c) reduces to

$$\left[\frac{-4\rho^6\left(\frac{\partial w}{\partial\rho}\right)^2+\rho^4\left(\delta^2\rho^2+\left(\frac{\partial w}{\partial\theta}\right)^2+\rho^2\left(\frac{\partial w}{\partial\rho}\right)\right)^2}{\delta^2\left(\delta^2\rho^2+\left(\frac{\partial w}{\partial\theta}\right)^2+\rho^2\left(\frac{\partial w}{\partial\rho}\right)^2\right)^3}-1\right]\frac{2C_1}{\Gamma}\frac{\partial^2 w}{\partial\rho^2}$$
$$+\left[\frac{-4\rho^5\delta^2-8\rho^4\left(\frac{\partial w}{\partial\theta}\right)\left(\frac{\partial^2 w}{\partial\theta\partial\rho}\right)-4\rho^5\left(\frac{\partial w}{\partial\rho}\right)^2}{\delta^2\left(\delta^2\rho^2+\left(\frac{\partial w}{\partial\theta}\right)^2+\rho^2\left(\frac{\partial w}{\partial\rho}\right)^2\right)^3}+\frac{5\rho^3}{\delta^2\left(\delta^2\rho^2+\left(\frac{\partial w}{\partial\theta}\right)^2+\rho^2\left(\frac{\partial w}{\partial\rho}\right)^2\right)^2}-\frac{1}{\rho}\right]+\frac{2C_1}{\Gamma}\frac{\partial w}{\partial\rho}$$
$$+\left[\frac{-4\rho^2\left(\frac{\partial w}{\partial\theta}\right)^2+\rho^2\left(\delta^2\rho^2+\left(\frac{\partial w}{\partial\theta}\right)^2+\rho^2\left(\frac{\partial w}{\partial\rho}\right)^2\right)}{\delta^2\left(\delta^2\rho^2+\left(\frac{\partial w}{\partial\theta}\right)^2+\rho^2\left(\frac{\partial w}{\partial\rho}\right)^2\right)^3}-\frac{1}{\rho^2}\right]\frac{2C_1}{\Gamma}\frac{\partial^2 w}{\partial\theta^2}-\frac{\partial^2 w}{\partial t^2}=0 \tag{31}$$

The accuracy of this hypothesis is corroborated in the following analysis.

To obtain the nonlinear response of the stretched membrane, the transversal displacement field is approximated by a sum of $M\times K$ natural modes:

$$w(\rho,\theta,t)=\sum_{m=1}^{M}\sum_{n=1}^{K}A_{mn}(t)J_n\left(\alpha_{mn}\frac{\rho}{R_o}\right)\cos(n\theta) \tag{32}$$

where $A_{mn}(t)$ are the time-dependent modal amplitudes.

The Galerkin method is applied so that the nonlinear partial differential equation of motion in the transversal direction, Eq. (31), is transformed into a system of $M\times K$ ordinary differential equations of motion in the time domain.

4.2.1. Nonlinear vibration results

The nonlinear free undamped vibrations ($p_h(t)=0$; $\zeta=0$), which are associated with the lowest natural frequency ($m=1$; $n=0$) and correspond to the first axi-symmetric mode, are first considered. The transversal displacement is approximated by expanding Eq. (32) with $K=0$ and an increasing number of radial modes ($M=1$, 2, and 3). The equations of motion are then solved using continuation techniques [67], and the frequency–amplitude relation is obtained. Fig. 7 shows the variation of each modal amplitude in Eq. (32) considering an increasing number of terms in the Galerkin approximation for a stretched membrane with $\delta=1.10$. The results indicate that a reduced model with only one degree of freedom ($M=1$) is sufficient to obtain the correct response up to very large deflections. The amplitudes of the subsequent modes (A_{20} and A_{30}) are rather small when compared to A_{10}. A reduced order model with only one degree of freedom may therefore be used to describe the frequency–amplitude relation up to very large deflections.

To evaluate the accuracy of the reduced order models, the amplitude–frequency relation is obtained using the finite element software Abaqus®. To do this, a mesh of 576 membrane elements, which is able to handle both the geometric and material nonlinearities, is used, and the response is obtained for a node on the undeformed membrane with the coordinates $(\rho,\theta)=(0.5,\ 0)$. A total of 1731 nonlinear equations of motion are numerically integrated, and the frequency–amplitude relation is obtained using the methodology proposed by Nandakumar and Chatterjee [68]: the time response of the slightly damped system is obtained for a chosen node, and the maximum amplitude and corresponding period between two consecutive positive peaks are computed at each cycle. Consider two successive peaks at times T_1 and T_2. Let their average value be A_1. Let the trough between these two positive peaks be A_2. We then define the amplitude as $A=(A_1-A_2/2)$, and the frequency as $\omega=1/(T_1-T_2)$. The resulting amplitude and frequency values are plotted to give the curve. A smaller number of finite elements was used here than in natural frequency analysis, because the convergence of the time response in our case can be attained with a less refined discretization, leading to less computational effort. The finite element formulation naturally takes into account the influence of the in-plane displacement and inertia forces, which are neglected in the theoretical model. The FE results are compared with the results of the reduced order models obtained for the same set of coordinates in Fig. 8. An excellent agreement between the two models is observed. For small vibration amplitudes, the response shows a strong increase in the natural frequency. As the vibration amplitude increases, the hardening effect decreases, and the curve veers upward tending to a constant frequency value for large vibration amplitudes.

Since the SDOF model compares well with the more refined modal solutions and with the FE results, this model is selected to perform a parametric analysis on the influence of the problem parameters on the nonlinear response.

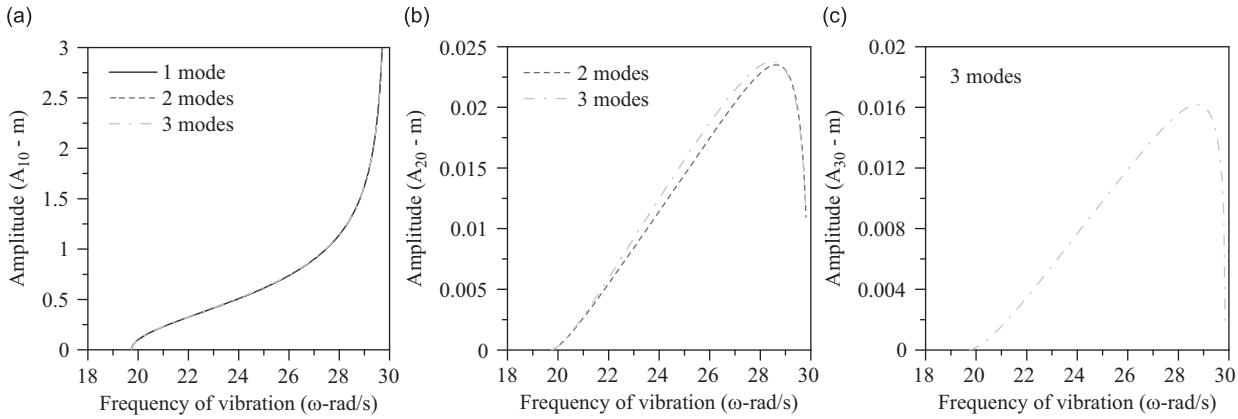

Fig. 7. Variation of the modal amplitudes A_{i0} as a function of the frequency, considering an increasing number of modes in Eq. (31). $\delta = 1.10$. (a) A_{10}; (b) A_{20}; (c) A_{30}.

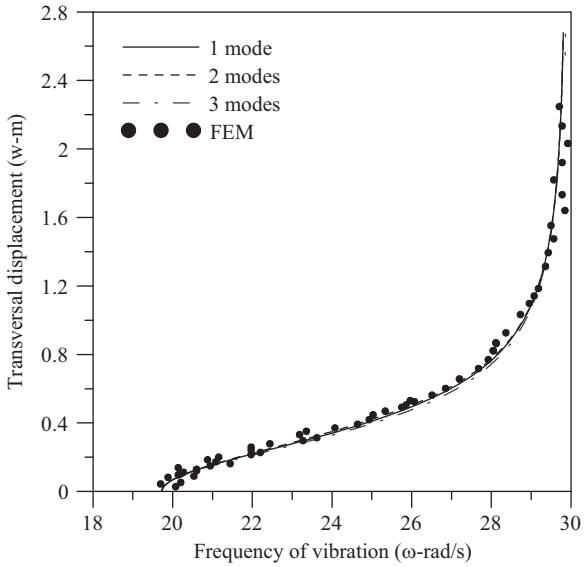

Fig. 8. Frequency–amplitude relation ($\delta = 1.10$). Transversal displacement w at a point $(\rho, \theta) = (0.5, 0)$.

Continuation algorithms are used to obtain all results, and Floquet theory is applied to ascertain the stability of the periodic solutions.

Fig. 9 illustrates the influence of the stretching ratio δ on the nonlinear frequency–amplitude relation. As the stretching ratio δ increases, the nonlinearity decreases, and the relation approaches linearity for $\delta > 2$. All curves converge asymptotically to the same value of ω as the vibration amplitude increase. By calculating the limit of the nonlinear equation of motion in the transversal direction, Eq. (24.c), as $\delta \to \infty$, one obtains the linear equation of motion equation (26). Both the natural frequency and the frequency–amplitude relation converge to same value of ω as δ increases. This value is given by Eq. (30). All frequencies depict the same nonlinear behavior observed here for $m = 1$ and $n = 0$. For a lightly tensioned membrane, the variation of the nonlinear frequency with the amplitude is rather strong. The variation between the natural (minimum) frequency and the maximum natural frequency, given by Eq. (30), is a function of δ only and is given by

$$\frac{\omega_{mn}(\infty)}{\omega_{mn}} = \sqrt{\frac{\delta^6}{\delta^6 - 1}} \tag{33}$$

For example, when $\delta = 1.02$, the variation of ω_{10} is of approximately 200%, as shown in Fig. 9. The characteristics of the curve can be explored for membrane sensor and actuator design [69].

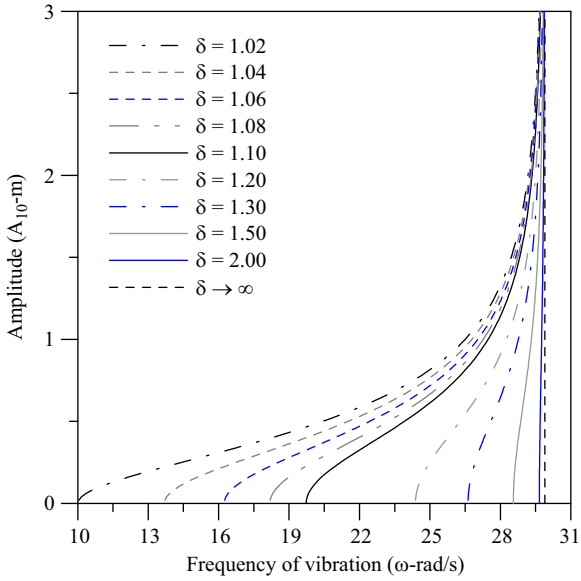

Fig. 9. Influence of the stretching ratio δ on the frequency–amplitude relation ($m = 1$, $n = 0$).

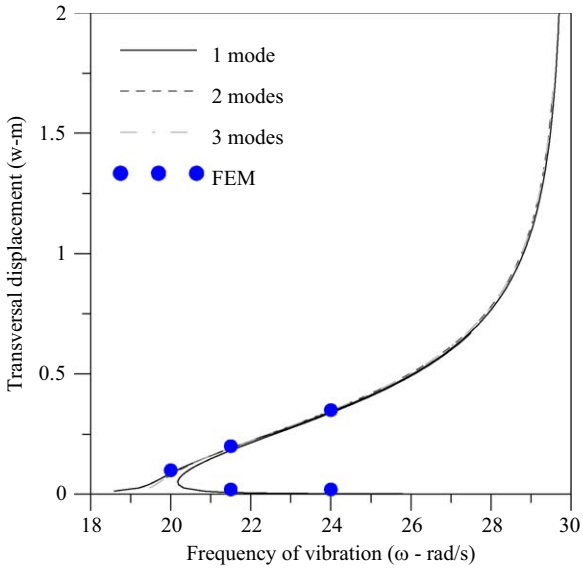

Fig. 10. Nonlinear resonance curve ($\delta = 1.10$).

The forced vibrations of the membrane are also considered. Fig. 10 shows the nonlinear resonance curve of the three reduced order models for $\delta = 1.10$ and an amplitude of excitation $P_o = 1$. In spite of the high degree of model nonlinearity, accurate results up to large deflections are clearly obtained. Additionally, the maximum amplitude of the steady-state response obtained by the FEM for selected values of the forcing frequency compare well with the present solution both for small and large vibration amplitudes. This can be explained, as shown previously, by the fact that the nonlinearity of the response decreases as the vibration amplitude increases, which lessens the importance of higher modes in the large amplitude response. This behavior is different from that of most structural elements, where the degree of nonlinearity increases with the vibration amplitude.

Fig. 11 shows the resonance curves of the pre-stretched membrane for stretching ratios varying from $\delta = 1.02$ to 2.00. All curves converge to the linear resonance curve as the vibration amplitude increases. As δ increases, the nonlinearity decreases, and is nearly linear for $\delta = 2.0$.

To gain insight into the nonlinear dynamic behavior of the membrane, the force response curves are obtained for different membrane parameter values. Fig. 12 shows, for selected values of the excitation frequency and $\delta = 1.10$, the

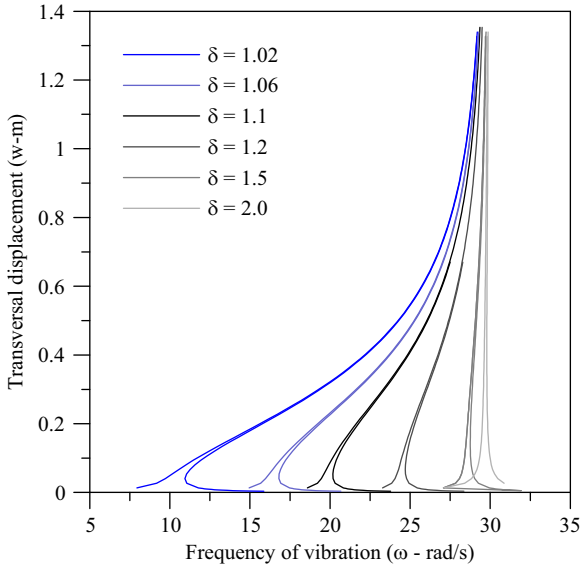

Fig. 11. Nonlinear resonance curves for increasing values of the stretching ratio δ.

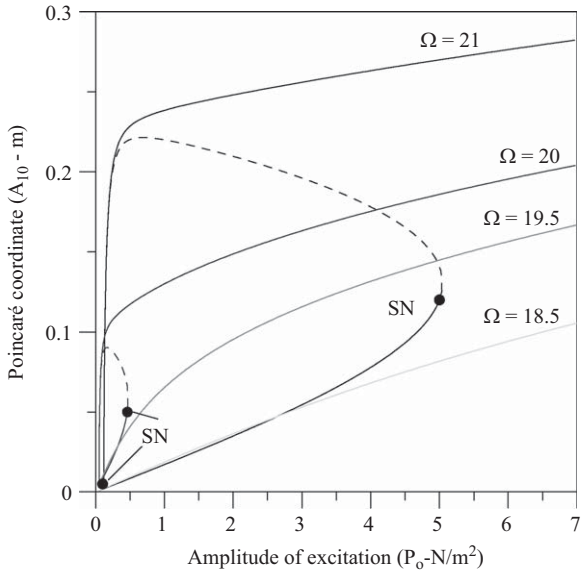

Fig. 12. Bifurcation diagrams for$\delta = 1.10$, $c = 0.05$ and selected values of the forcing frequency Ω.

bifurcation diagrams as a function of the forcing amplitude P_o. In Fig. 12 and henceforth, dashed lines represent unstable responses, while continuous lines represent stable responses. Depending on the value of P_o and Ω, the membrane may display either one or three responses. For example, for an excitation frequency $\Omega = 21$, which is near the lowest natural frequency, there are two stable and one unstable solution for a large range of P_o. The stable and unstable branches are connected by saddle-node bifurcations where one Floquet multiplier crosses the unit circle through +1 (SN in the figures). For values of the excitation frequency away from the resonance region, only one response (stable) is observed.

Fig. 13, where the coordinate of the Poincaré map A_{10} is plotted as a function of the excitation frequency, shows the bifurcation diagrams for three different values of the stretching ratio δ. In each case, two saddle-node bifurcations are observed. As the stretching ratio increases, the nonlinearity of the response decreases, decreasing the frequency range where unstable solutions exist, as expected. Fig. 14 shows bifurcation diagrams with the magnitude of the forcing P_o as the control parameter, and increasing values of the stretching ratio δ. In each case, the forcing frequency is chosen in the main resonance region of the hardening system, just to the right of the natural frequency of the pre-stretched membrane. This is the region where nonlinear effects are most important. As before, one can observe the decreasing influence of the

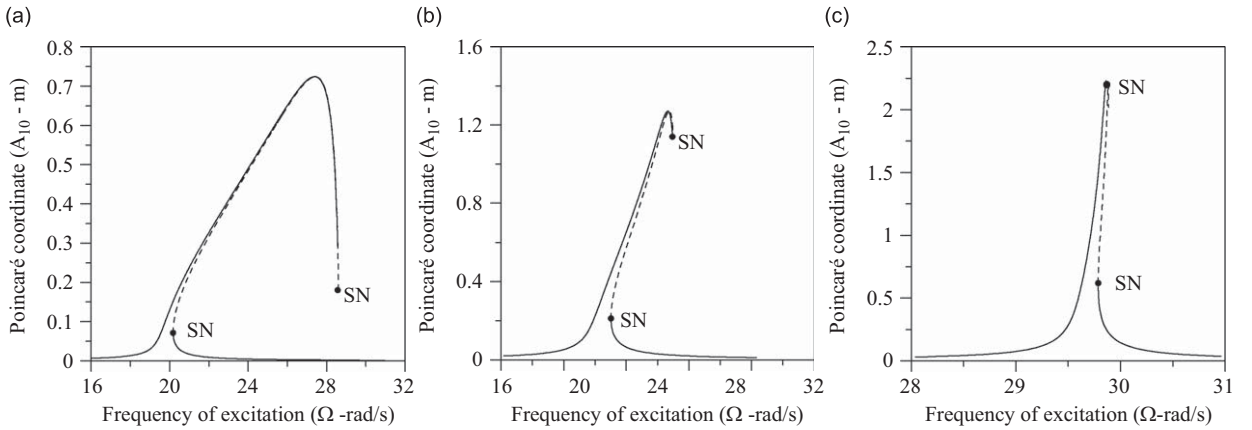

Fig. 13. Bifurcation diagrams for increasing pre-stretching ratios. Coordinate A_{10} as a function of the excitation frequency Ω ($P_o = 1$; $c = 0.05$). (a) $\delta = 1.10$; (b) $\delta = 1.50$; (c) $\delta = 2.0$.

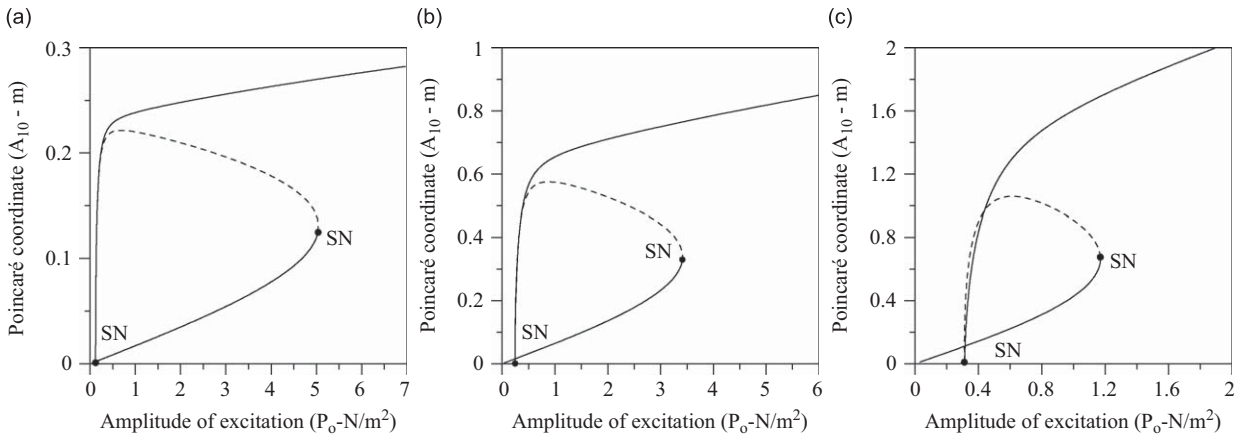

Fig. 14. . Bifurcation diagrams for selected values of the excitation frequency, Ω and stretching ratio δ. Coordinate A_{10} as a function of the forcing amplitude P_o. $c = 0.05$. (a) $\Omega = 21$; $\delta = 1.10$; (b) $\Omega = 29$; $\delta = 1.50$; (c) $\Omega = 29.8$; $\delta = 2.00$.

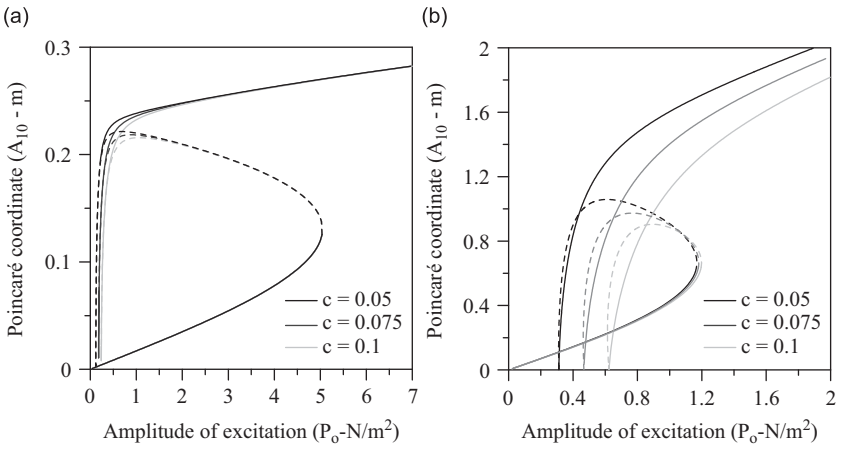

Fig. 15. Influence on the damping coefficient c on the non-linear behavior and stability of the membrane. $P_o = 1$. (a) $\delta = 1.1$; $\Omega = 21$; (b) $\delta = 2.0$; $\Omega = 29.8$.

nonlinearity with increasing radial stretching. The influence of the damping ratio is illustrated in Fig. 15, where bifurcation diagrams are obtained for two values of the radial stretching ratio and increasing values of the damping coefficient. The influence damping increases as the stretching ratio increases. The damping reduces the multiplicity solution region and jumps where co-existing stable solutions may occur.

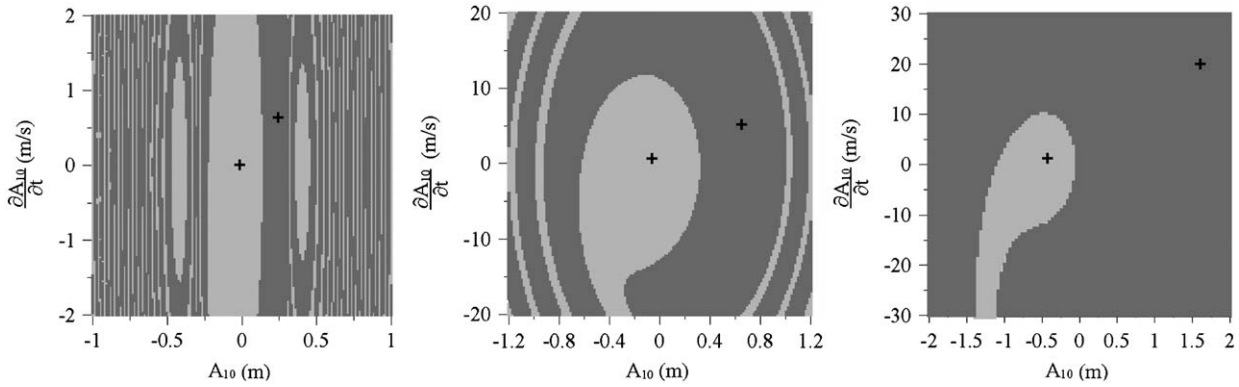

Fig. 16. Basins of attraction for selected values of the control parameters. ($c = 0.05$). (a) $\delta = 1.1$; $P_o = 1$; $\Omega = 21$; (b) $\delta = 1.5$; $P_o = 1.5$; $\Omega = 29$; (c) $\delta = 2.0$; $P_o = 1$; $\Omega = 29.8$. Dark gray: basin of attraction of the resonant large amplitude oscillation. Light gray: Basin of attraction of the small amplitude oscillation. Black cross: fixed point of the Poincaré Map (attractor).

The influence of the system and force parameters on the degree of nonlinearity of the membrane response can also be observed in the topological complexity of the basin of attraction. Fig. 16 illustrates the basin of attraction of the membrane for three sets of parameters. The parameters are chosen in such a way that the response lies in the main resonance region where three solutions occur: one unstable medium amplitude solution, one stable small amplitude solution, and one stable large amplitude solution. The dark gray color corresponds to the basin of attraction of the resonant large amplitude oscillation, while light gray corresponds to the basin of attraction of the small amplitude oscillation. A black cross denotes the two attractors. As the radial stretching ratio increases, the complexity of the basin topology decreases with a smaller number of light and dark gray bands. It is interesting to note that in the main resonance region, most initial conditions lead to solutions that converge to the large amplitude attractor.

5. Influence of constitutive law

There are several examples in the literature of the use of constitutive laws for the modeling of hyperelastic rubber-like materials characterized by large strains and the absence of irreversible strains during the loading–unloading cycles. The aim of this section is to compare the different constitutive models. Thus, the constitutive equations must be fitted for each material using appropriate experimental data. Here, the reference data correspond to the stress–strain relation obtained experimentally for the membrane analyzed in Ref. [27], and shown in Fig. 4 of the referred paper.

There are several constitutive laws in the literature particularly adapted to the representation of elastomers based on strain invariants. Rivlin [70] has proposed the following polynomial form for the energy density function

$$w = \sum_{m,n} C_{mn}(I_1 - 3)^m (I_2 - 3)^n \tag{34}$$

also known as the Mooney–Rivlin strain-energy density function, because the first-order polynomial function

$$w = C_1(I_1 - 3) + C_2(I_2 - 3) \tag{35}$$

which was first been introduced by Mooney [71]. Eq. (35) is a function of two constants, C_1 and C_2. This is probably one of the most used strain densities in the literature. The neo-Hookean strain density function can be considered as a special case of Eq. (35) with $C_2 = 0$.

The constitutive model for incompressible hyperelastic materials proposed by Yeoh [25] assumes that the strain energy is a power series of the term (I_1–3), being a generalization of the neo-Hookean model. It is thus written as

$$W = \sum_{i=1}^{N} C_i (I_1 - 3)^i \tag{36}$$

where N is the number of terms in the series and C_i are material parameters.

Arruda and Boyce [26] proposed the following constitutive law for rubber-like materials:

$$W = \mu\left\{\frac{(I_1-3)}{2} + \frac{(I_1^2-9)}{20\lambda_m^2} + \frac{11(I_1^3-27)}{1050\lambda_m^4} + \frac{19(I_1^4-81)}{7000\lambda_m^6} + \frac{519(I_1^5-243)}{673750\lambda_m^8}\right\} \tag{37}$$

where μ and λ_m are the constants of the material.

Another constitutive law is found in Ogden [23,24], which is based on the experimental results obtained for rubber-like materials by Treolar [39]. In this case the strain-energy density function is given by

$$w = \sum_{n=1}^{3} \frac{\mu_n(\lambda_1^{\alpha_n} + \lambda_2^{\alpha_n} + \lambda_3^{\alpha_n} - 3)}{\alpha_n} \tag{38}$$

where λ_i are the extensions in the principal directions, and μ_n and α_n are material parameters.

In order to establish the constants for each constitutive law, the experimental stress–strain curve given in [27] and used for the determination of the neo-Hookean constitutive law is supplied to the FE program Abaqus®, and the material constants for each constitutive model are calculated using an error minimization procedure (given in Table 2). The three lowest natural frequencies obtained for each model are given in Table 3 and compared with the neo-Hookean theoretical results obtained from Eq. (29). They give almost identical results. The largest difference is obtained for the Ogden model. The stress–strain curve for each model is shown in Fig. 17. The frequency–amplitude relation is then obtained for each constitutive law, and using the methodology proposed by Nandakumar and Chatterjee [68] as explained in Section 4. For the numerical analysis, 576 membrane elements are used, which gives 1731 equations of motion. The results are compared with the solution obtained using the neo-Hookean constitutive law in Fig. 17 for a stretching ratio $\delta = 1.10$. The membrane gives the same overall behavior independent of the adopted constitutive law (Fig. 18).

Table 2
Elastic constants for each constitutive law.

Neo-Hookeano	$C_1 = 170000$ Pa		
Mooney–Rivlin	$C_1 = 169720.3$ Pa	$C_2 = -18.7$ Pa	
Yeoh ($N = 3$)	$C_1 = 163694.04$ Pa	$C_2 = 209$ Pa	$C_3 = -1.84$ Pa
Arruda–Boyce	$\mu = 331373.66$ Pa	$\lambda_m = 18$	
Ogden	$\mu_1 = 1279517.5$ Pa	$\alpha_1 = 1.47875$	
	$\mu_2 = -16902.5$ Pa	$\alpha_2 = 1.90802$	
	$\mu_3 = -949448.8$ Pa	$\alpha_3 = 1.07815$	

Table 3
Linear vibration frequencies (rad/s).

$\delta = 1.10$										
m	n	Neo-Hookeano	Mooney-Rivlin	%	Yeoh ($N = 3$)	%	Arruda–Boyce	%	Ogden	%
1	0	19.771	19.754	0.086	19.404	1.856	19.538	1.178	18.699	5.422
1	1	31.412	31.384	0.089	30.827	1.862	31.040	1.184	29.708	5.424
1	2	41.817	41.780	0.088	41.040	1.858	41.323	1.181	39.550	5.421

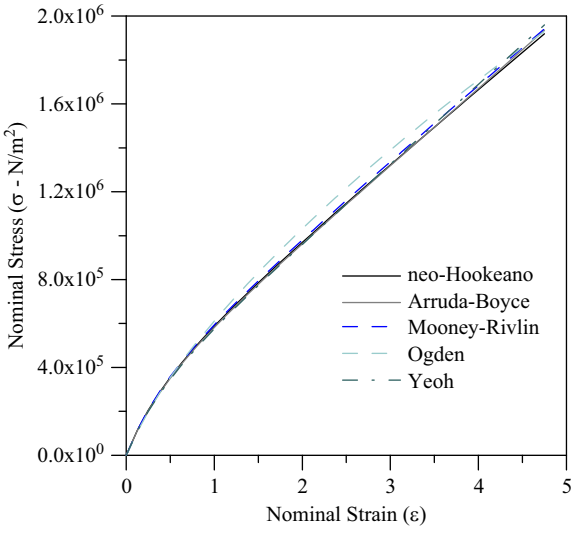

Fig. 17. Stress–strain curves obtained by various models using the same experimental data [27].

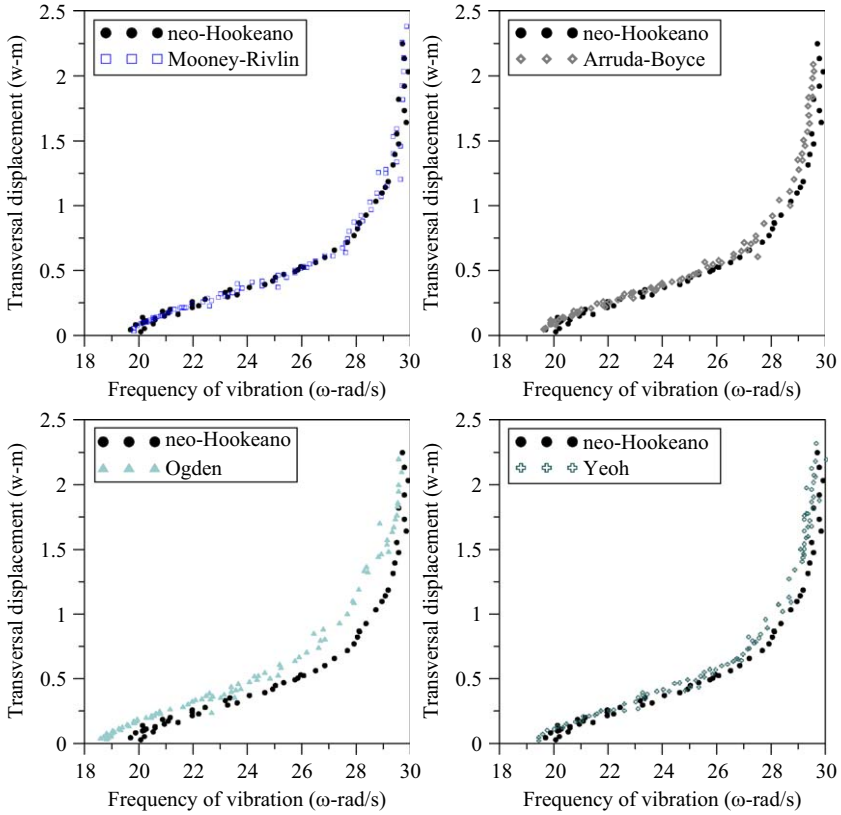

Fig. 18. Frequency–amplitude relation for mode $n = 0$ and $m = 1$ and $\delta = 1.10$. The transversal displacement w is measured at a node with coordinates $(\rho, \theta) = (0.5, 0)$.

6. Conclusions

The mathematical modeling for the nonlinear vibration analysis of a pre-stretched hyperelastic membrane under finite deformations is presented. The membrane material is considered to be homogeneous, isotropic, and neo-Hookean. First, the exact solution of the stretched membrane is obtained, which shows that all relevant quantities are a function of the material constant and the stretching ratio in the radial direction (deformed radius/undeformed radius) only. The equations of motion of the stretched membrane are then obtained. By analytically solving the linearized equations of motion, the vibration modes and frequencies of the hyperelastic membrane are obtained, and these normal modes are used, together with the Galerkin method, to obtain low-order approximations of the nonlinear dynamic response. The same problem is also analyzed using the finite element software Abaqus®. The results show that an sdof model can give accurate results up to very large deflections. The accuracy of this low-order model is verified via comparisons with the higher order modal approximations, and the numerical values are computed by the finite element method, which compare rather well with the theoretical results. The results highlight the influence of the stretching ratio on the vibration frequencies, nonlinear frequency–amplitude relation, and bifurcation diagrams. It is shown that a lightly stretched membrane displays a highly nonlinear response, that the nonlinearity decreases as the stretching ratio increases, and the response becomes practically linear for a deformed radius of twice the initial value. Both the frequency–amplitude relation and the corresponding linear frequency converge to the same frequency upper bound as the radial stretch and/or vibration amplitude increases. This explains the accuracy of the low-order models for large finite amplitude oscillations of the hyperelastic membrane. Finally, the membrane is analyzed using different invariant-based constitutive models, including the Mooney–Rivlin, Yeoh, Ogden, and Arruda–Boyce models. The results show that the membrane exhibits the same non-linear frequency–amplitude relation for all tested models. Therefore, due to its high accuracy, the present formulation and theoretical results may serve as important patch tests for guiding the development of fully nonlinear numerical and analytical models that can address more complex geometries and boundary conditions.

Acknowledgments

The authors acknowledge the financial support of the Brazilian research agencies CAPES, CNPq and FAPERJ.

References

[1] C.H. Jenkins, J.W. Leonard, Nonlinear dynamic response of membranes: state of the art, *ASME Applied Mechanics Reviews* 44 (1991) 319–328.
[2] C.H. Jenkins, *Gossamer Spacecraft: Membrane and Inflatable Structures Technology for Space Applications*, AIAA, Reston, VI, USA, 2001.
[3] C.H. Jenkins, U. Korde, A. Membrane, Vibration experiments: an historical review and recent results, *Journal of Sound and Vibration* 295 (2006) 602–613.
[4] Y.C. Fung, *Biomechanics: Motion, Flow, Stress, and Growth*, Springer, New York, 1990.
[5] J.D. Humphrey, *Cardiovascular Solid Mechanics: Cells, Tissues, and Organs*, Springer, New York, 2002.
[6] C. Poilane, P. Delobell, C. Lexcellent, S. Hayashi, H. Tobushi, Analysis of the mechanical behavior of shape memory polymer membranes by nanoindentation, bulging and point membrane deflection tests, *Thin Solid Films* 379 (2000) 156–165.
[7] Y. Liang, Y. Kuga, M. Taya, Design of membrane actuator based on ferromagnetic shape memory alloy composite for synthetic jet applications, *Sensors and Actuators A: Physical* 125 (2006) 512–518.
[8] R. Pelrine, R. Kornbluh, Q. Pei, J. Joseph, High-speed electrically actuated elastomers with strain greater than 100%, *Science* 287 (2000) 836–839.
[9] J.W. Fox, N.C. Goulbourne, On the dynamic electromechanical loading of dielectric elastomer membranes, *Journal of the Mechanics and Physics of Solids* 56 (2008) 2669–2686.
[10] S. Bauer, M. Paajanen, Electromechanical characterization and measurement protocol for dielectric elastomer actuators, in: Proceedings of SPIE, Smart Structures and Materials on Electroactive Polymers and Devices, San Diego, 2006, pp. 6168–61682K.
[11] N.C. Goulbourne, E.M. Mockensturm, M. Frecker, A nonlinear model for dielectric elastomer membranes, *ASME Journal of Applied Mechanics* 72 (2005) 899–906.
[12] Z. Suo, X. Zhao, W.H. Greene, A nonlinear field theory of deformable dielectrics, *Journal of the Mechanics and Physics of Solids* 56 (2008) 467–486.
[13] D.D. Shin, K.P. Mohanchandra, G.P. Carman, Development of hydraulic linear actuator using thin film SMA, *Sensors and Actuators A: Physical* 119 (2005) 151–156.
[14] M. Wissler, E. Mazza, Mechanical behavior of an acrylic elastomer used in dielectric elastomer actuators, *Sensors Actuators A: Physical* 134 (2007) 494–504.
[15] K. Pope, Pressure–volume characteristics of dielectric elastomer laminates for blood pump applications, Master of Science, Pennsylvania State University, Hershey, 2004.
[16] N. Goulbourne, M. Frecker, E. Mockensturm, Electro-elastic modeling of a dielectric elastomer diaphragm for a prosthetic blood pump, in: Proceedings of SPIE, Smart Structures and Materials on Electroactive Polymers and Devices, San Diego, 2004, pp. 122–133.
[17] P.B. Goncalves, D. Pamplona, P.B.C. Teixeira, R.L.C. Jerusalmi, I.A. Cestari, A.A. Leirner, Dynamic non-linear behavior and stability of a ventricular assist device, *International Journal of Solids and Structure* 40 (2003) 5017–5035.
[18] R.S. Rivlin, Large elastic deformations of isotropic materials, *Philosophical Transactions of the Royal Society* A240 (1948) 459–491.
[19] G.I. Barenblatt, D.D. Joseph (Eds.), *Collected Papers of R.S. Rivlin*, Vols. I and II, Springer, 1996.
[20] A.E. Green, J.E. Adkins, *Large Elastic Deformations and Non-Linear Continuum Mechanics*, Oxford University Press, Oxford, 1960.
[21] A. Libai, J.G. Simmonds, *The Nonlinear Theory of Elastic Shells*, 2nd ed., Cambridge University Press, Cambridge, 1998.
[22] Y.B. Fu, R.W. Ogden, *Nonlinear Elasticity—Theory and Applications, London Mathematical Society*, Cambridge University Press, Cambridge, 2001 (Lecture Notes Series 283).
[23] R.W. Ogden, Large deformation isotropic elasticity on the correlation of theory and experiment for incompressible rubber-like solids, *Proceedings of the Royal Society of London*, vol. A326, London, 1972, pp. 565–584.
[24] R.W. Ogden, *Non-linear Elastic Deformations*, Ellis Horwood Ltd., Chichester, 1984.
[25] O.H. Yeoh, Some forms of the strain energy function for rubber, *Rubber Chemistry and Technology* 66 (1993) 754–771.
[26] E.M. Arruda, M.C. Boyce, A three-dimensional constitutive model for the large stretch behaviour of rubber elastic materials, *Journal of the Mechanics and Physics of Solids* 41 (1993) 389–412.
[27] A.P.S. Selvadurai, Deflections of a rubber membrane, *Journal of the Mechanics and Physics of Solids* 54 (2006) 1093–1119.
[28] G. Saccomandi, R.W. Ogden, *Mechanics and Thermomechanics of Rubberlike Solids*, Springer, Wien, 2004 (CISM Courses and Lectures No. 452).
[29] D. Pamplona, C.R. Calladine, The mechanics of axially symmetric liposomes, *Journal of Biomechanical Engineering* 115 (1993) 149–159.
[30] M.L. Raghavan, D.A. Vorp, Toward a biomechanical tool to evaluate rupture potential of abdominal aortic aneurysm: identification of a finite strain constitutive model and evaluation of its applicability, *Journal of Biomechanics* 33 (2000) 475–482.
[31] D.M. Haughton, Elastic membranes, in: Y.B. Fu, R.W. Ogden (Eds.), *Nonlinear Elasticity: Theory and Applications*, Cambridge University Press, Cambridge, 2001 (Chapter 7).
[32] D. Pamplona, P.B. Gonçalves, M. Davidovich, H.I. Weber, Finite axisymmetric deformations of an initially stressed fluid-filled cylindrical membrane, *International Journal of Solids and Structures* 38 (2001) 2033–2047.
[33] A.N. Gent, Elastic instabilities in rubber, *International Journal of Non-Linear Mechanics* 40 (2005) 165.
[34] D. Pamplona, P.B. Gonçalves, S.R.X. Lopes, Finite deformations of cylindrical membranes under internal pressure, *International Journal of Mechanical Sciences* 48 (2006) 683–696.
[35] Y.B. Fu, S.P. Pearce, K.K. Liu, Post-bifurcation analysis of a thin-walled hyperelastic tube under inflation, *International Journal of Non-Linear Mechanics* 43 (2008) 697–706.
[36] R.S. Rivlin, D.W. Saunders, Large elastic deformations of isotropic materials. VII. Experiments on the deformation of rubber, *Philosophical Transactions of the Royal Society* A243 (1951) 251–288.
[37] F.S. Wong, R.T. Shield, Large plane deformations of thin elastic sheets of neo-Hookean material, *Journal of Applied Mathematics and Physics* 20 (1969) 176–199.
[38] P.D.S. Verna, O.H. Rana, Radial deformations of a plane sheet containing a circular hole or inclusion, *International Journal of Non-Linear Mechanics* 13 (1978) 223–232.
[39] L.R.G. Treloar, Strains in an inflated rubber sheet, and the mechanism of bursting, *Institution of the Rubber Industry Transactions* 19 (1944) 201–212.
[40] J.E. Adkins, R.S. Rivlin, Large elastic deformations of isotropic materials IX. The deformation of thin shells, *Philosophical Transactions of the Royal Society of London* A244 (1952) 505–531.
[41] J.D. Campbell, On the theory of initially tensioned circular membranes subjected to uniform pressure, *Quarterly Journal of Mechanics and Applied Mathematics* (1956) 84–93.
[42] W.W. Klingbeil, R.T. Shield, Some numerical investigations on empirical strain energy functions in the large axisymmetric extensions of rubber membranes, *Journal of Applied Mathematics and Physics* 15 (1964) 608–629.
[43] L.J. Hart-Smith, J.D.C. Crisp, Large elastic deformations of thin rubber membranes, *International Journal of Engineering Science* 5 (1967) 1–24.
[44] Foster, Inflation of a plane circular membrane, *Journal of Engineering for Industry* 89 (1967) 403–407.
[45] J.T. Tielking, W.W. Feng, The application of the minimum potential energy principle to nonlinear axisymmetric membrane problems, *Journal of Applied Mechanics* 41 (1974) 491–496.
[46] A. Wineman, D. Wilson, J.W. Melvin, Material identification of soft tissue using membrane inflation, *Journal of Biomechanics* 12 (1979) 841–850.
[47] P.A. Przybylo, E.M. Arruda, Experimental investigations and numerical modeling of incompressible elastomers during nonhomogeneous deformations, *Rubber Chemistry and Technology* 71 (1998) 730–749.
[48] Y. Li, J.A. Nemes, A.A. Derdouri, Membrane inflation of polymeric materials: experiments and finite element simulations, *Polymer Engineering and Science* 41 (2001) 1399–1412.

[49] M. Rachik, F. Schmidt, N. Reuge, Y. Le Maoult, F. Abbe, Elastomers biaxial characterization using bubble inflation technique. II: numerical investigation of some constitutive models, *Polymer Engineering and Science* 41 (2001) 532–541.
[50] A. Wineman, J. Shaw, Influence of thermally induced scission and crosslinking on the post-scission inflation of circular elastomeric membranes, *International Journal of Engineering Science* 46 (2008) 758–774.
[51] S.J. Farlow, *Partial Differential Equations for Scientists and Engineers*, Dover Publications, New York, 1993.
[52] C.Y. Wang, Vibration of an annular membrane attached to a free, rigid core, *Journal of Sound and Vibration* 260 (2003) 776–782.
[53] G.R. Buchanan, Vibration of circular membrane with linearly varying density along a diameter, *Journal of Sound and Vibration* 280 (2005) 407–441.
[54] N. Akkas, On the dynamic snap-out instability of inflated non-linear spherical membranes, *International Journal of Non-Linear Mechanics* 13 (1978) 177–183.
[55] E. Verron, R.E. Khayat, A. Derdouri, B. Peseaux, Dynamic inflation of hyperelastic spherical membranes, *Journal of Rheology* 43 (1999) 1083–1097.
[56] U. Akyüz, A. Ertepinar, Stability and asymmetric vibrations of pressurized compressible hyperelastic cylindrical shells, *International Journal of Non-Linear Mechanics* 34 (1999) 391–404.
[57] V.H. Tuzel, H.A. Erbay, The dynamic response of an incompressible non-linearly elastic membrane tube subjected to a dynamic extension, *International Journal of Non-Linear Mechanics* 39 (2004) 515–537.
[58] E.M. Mockensturm, N. Goulbourne, Dynamic response of dielectric elastomers, *International Journal of Non-Linear Mechanics* 41 (2006) 388–395.
[59] L. Jiang, J.B. Haddow, J.L. Wegner, The dynamic response of a stretched circular hyperelastic membrane subjected to normal impact, *Wave Motion* 16 (1992) 137–150.
[60] L. Jiang, Application of the Taylor–Galerkin finite element and Godunov-type finite difference methods to finite amplitude axisymmetric waves in hyperelastic membranes, *Journal of Sound and Vibration* 192 (1996) 223–244.
[61] R.E. Khayat, A. Derdouri, Stretch and inflation of hyperelastic membranes as applied to blow molding, *Polymer Engineering and Science* 35 (1995) 1852–1863.
[62] H.W. Haslach, J.D. Humphrey, Dynamics of biological soft tissue and rubber: internally pressurized spherical membranes surrounded by a fluid, *International Journal of Non-Linear Mechanics* 39 (2004) 399–420.
[63] R. Jiusheng, Dynamics and destruction of internally pressurized incompressible hyper-elastic spherical shells, *International Journal of Engineering Science* 47 (2009) 745–753.
[64] Abaqus version 6.5 Standard User's Manual, Hibbitt, Karlsson, and Sorensen Inc., Pawtucket, USA, 2001.
[65] L.R.G. Treloar, *Physics of Rubber Elasticity*, 3rd ed., University Press, Oxford, 1975.
[66] D. Fischer, Configuration dependent pressure potentials, *Journal of Elasticity* 19 (1988) 77–84.
[67] E. Allgower, K. Georg, *Numerical Continuation Methods. An Introduction*, Springer, Berlin, 1990.
[68] K. Nandakumar, A. Chatterjee, Resonance, parameter estimation, and modal interactions in a strongly nonlinear Benchtop oscillator, *Nonlinear Dynamics* 40 (2005) 149–167.
[69] Miao Yu, Xinhua Long, B. Balachandran, Sensor diaphragm under initial tension: nonlinear responses and design implications, *Journal of Sound and Vibration* 312 (2008) 39–54.
[70] R.S. Rivlin, Large elastic deformations of isotropic materials: I. Fundamental concepts. II. Some uniqueness theorems for pure homogeneous deformation, *Philosophical Transactions of the Royal Society of London* A240 (1948) 459–508.
[71] M. Mooney, A theory of large elastic deformations, *Journal of Applied Physics* 11 (1940) 582–592.